Understanding the Genesis of Cardiac Signals in Electrical Impedance Tomography

M. Proença[1], F. Braun[1], M. Lemay[1], B. Grychtol[2], M. Bührer[3], M. Rapin[1], P. Krammer[4], S. Böhm[4], J. Solà[1] and J.-Ph. Thiran[5, 6]

[1]*Systems Division, Swiss Center for Electronics and Microtechnology (CSEM), Neuchâtel, Switzerland*
[2]*Division of Medical Physics in Radiology, German Cancer Research Center (DKFZ), Heidelberg, Germany*
[3]*Institute for Biomedical Engineering, University and ETH Zurich, Zurich, Switzerland*
[4]*Swisstom AG, Landquart, Switzerland*
[5]*Signal Processing Laboratory (LTS5), Swiss Federal Institute of Technology (EPFL), Lausanne, Switzerland*
[6]*Department of Radiology, University Hospital Center (CHUV) and University of Lausanne (UNIL), Lausanne, Switzerland*

Keywords: Electrical Impedance Tomography, EIT, Cardiac, Pulsatility, Perfusion, Origin, Genesis, Source.

Abstract: Electrical impedance tomography (EIT) is a safe and low-cost imaging technology allowing the monitoring of ventilation. While most EIT studies have investigated respiration-related events, EIT-based cardiovascular applications have received increasing attention over the last years only. Variations in intra-thoracic blood volume induce impedance changes that can be monitored with EIT and used for the estimation of hemodynamic parameters. There is, however, increasing evidence that variations in blood volume are not the only factors contributing to cardiac impedance changes within the heart. The mechanical action of the myocardium and movement of the heart-lung interface are suspected to generate impedance changes of non-negligible amplitude. To test this hypothesis we designed a dynamic 2D bio-impedance model from segmented human magnetic resonance data. EIT simulations were performed and showed that EIT signals in the heart area might be dominated up to 70% by motion-induced impedance changes.

1 INTRODUCTION

Electrical impedance tomography (EIT) is a non-invasive, non-ionizing and low-cost functional imaging technique allowing real-time visualization of impedance changes within the thorax. Its typical monitoring system consists in a belt of electrodes attached around the subject's chest. Small alternating electrical currents are injected in a sequential pattern. Simultaneous voltage measurements are performed on the non-injecting electrodes and are then fed in an image reconstruction algorithm.

With anatomical structures such as the lungs, filled with air (low conductivity), and the heart and blood vessels, filled with blood (high conductivity), EIT can assess intra-thoracic ventilation and perfusion distributions (Holder, 2005). While some commercial EIT devices (such as the Dräger PulmoVista® 500 monitor or, more recently, Swisstom's EIT Pioneer Set) exist and allow the monitoring of ventilation, the diagnosis of respiration-related disorders and the estimation of hemodynamic parameters via EIT still remain limited to the field of research.

1.1 Cardiac EIT

While research in EIT is mostly dedicated to ventilation – see (Bayford, 2006) for a review –, numerous studies have been carried out to evaluate the potential of EIT for the measurement of cardiogenic impedance variations, be it for the assessment of cardiac hemodynamics (Brown, 1992; Vonk-Noordegraaf, 2000; Grant, 2011) or lung perfusion (Smit, 2004; Frerichs, 2009; Borges, 2011).

EIT produces image sequences of low spatial but high temporal resolution. Frame rates as high as 50 images per second are common. It is thus possible to visualize – for each pixel in the image sequence – the temporal impedance variations occurring at its

Proença M., Braun F., Lemay M., Grychtol B., Bührer M., Rapin M., Krammer P., Böhm S., Solà J. and Thiran J..
Understanding the Genesis of Cardiac Signals in Electrical Impedance Tomography.
DOI: 10.5220/0004793400270034
In *Proceedings of the International Conference on Bio-inspired Systems and Signal Processing* (BIOSIGNALS-2014), pages 27-34
ISBN: 978-989-758-011-6

corresponding location. The impedance signal observed is typically composed of the superposition of a component at the respiratory frequency and another component at the cardiac frequency, of much smaller amplitude (typically less than 5% of the respiratory component) (Barber, 1990).

Various methods have been proposed in the literature to separate these two components. The most common one consists in exploiting the synchrony of cardiac EIT pulsatile signals with the electrocardiogram (ECG). Using ECG as a cardiogenic trigger, hundreds of cardiac cycles can be aligned and averaged to produce one representative impedance waveform where the influence of the respiratory component is strongly reduced (McArdle, 1988). Alternative methods consist in filtering the respiratory component out of the impedance signal, usually well separated from the cardiac component in the frequency domain (Leathard, 1994), or more recently by exploiting principal component analysis (Deibele, 2008). Although not appropriate for continuous monitoring in contexts such as intensive care units, asking the subject to hold his/her breath for a few seconds remains the simplest and most effective approach (Frerichs, 2002).

Thorough analysis of the spatial distribution of the respiratory and cardiac components in EIT image sequences allows the identification of thoracic functional structures, such as the heart and lungs, contained within the EIT electrode plane (Ferrario, 2012). With the respiratory component removed, pixel-wise impedance signals depict cardiac-related changes and can thus be processed for hemodynamic parameters estimation and EIT-based cardiac applications.

1.2 Controversial Origin of Cardiac-related Signals

At each heartbeat, a certain amount of blood known as stroke volume is ejected into both the systemic and pulmonary circulations. These blood volume displacements, along with the distensibility of the vessels and the motion of the heart, generate impedance variations at the cardiac frequency. Dissociating these various sources of *pulsatility*, or even quantifying their respective influence, is not trivial. Yet the exploitation of cardiac-related signals in EIT for studying hemodynamics depends on solving this issue.

The very nature of EIT itself becomes a challenging aspect when it comes to the interpretation of cardiac-related signals. For instance, from the EIT transverse plane view, structures such as the atria can hardly be discriminated from the ventricles (Vonk-Noordegraaf, 2000). Moreover, the diffusive nature of electrical currents several centimetres above and below the electrode plane makes the interpretation of EIT pixel-wise signals complex (Borges, 2011). For example, a pixel located in the posterior region of the heart could possibly undergo changes in impedance originating from the atria, the ventricles, the aorta and/or the pulmonary arteries, as well as pulmonary perfusion and heart motion. In addition to this puzzle, the well-known anatomical distortions of impedance tomograms make the localization – and thus the understanding – of cardiac-related impedance changes even more challenging (Barber, 1990).

1.2.1 Lung Pulsatility

All these difficulties do not just concern the monitoring of functional cardiac activity. In their review, Nguyen *et al.* quote numerous studies that have tackled the challenge that represents lung perfusion via EIT (Nguyen, 2012). However, uncertainties remain. In particular, the influence of the heart's motion on the lungs at the heart-lung interface remains one of the main sources of confusion (Frerichs, 2009). The unclear nature of cardiac-related impedance changes taking place within the lungs requires the use of a term more neutral than perfusion, such as lung pulsatility (Hellige, 2011).

Removing or isolating heart motion-induced impedance changes is challenging. Many studies, such as (Kunst, 1998; Vonk-Noordegraaf, 1998; Smit, 2004), have tried to minimize the effects of the motion of the heart on pulmonary pulsatility by measuring EIT at the level of the third intercostal space in human subjects with their arms stretched above their head. However, this configuration is not only unphysiologic and impractical for intensive care or long-term monitoring, it has also been shown to fail to suppress the influence of the heart's motion occasionally. These mechanical perturbations could also be the source of inconsistencies between several studies regarding the genesis of pulsatile signals in EIT. For instance, Smit *et al.* reported that the magnitude of the pulsatile signals in the lungs was only dependent on the size of the pulmonary microvascular bed – or, alternatively, on the distensibility of pulmonary vessels – but not on stroke volume (Smit, 2004). However, Fagerberg *et al.* reported significant correlations with stroke

volume, concluding that vessel distensibility only plays a minor role in the genesis of pulmonary pulsatility (Fagerberg, 2009). Additional contradictions regarding the origin of cardiac-related signals in EIT have recently been highlighted (Braun, 2013). Cardiac and pulmonary regions showing high pulsatility energy did not spatially match the passage of an impedance contrast agent (hypersaline solution), suggesting that the heart's motion could be affecting significantly cardiac EIT signals.

1.2.2 The Need for a Dynamic Model

In order to provide new insights to these unanswered questions, we designed a novel experiment based on the hypothesis that cardiac impedance changes in EIT are not only blood volume-related but also motion-induced. Testing this hypothesis as well as localizing and quantifying these mechanical perturbations requires the use of a *dynamic* bio-impedance model. To that end, we developed an anatomically-consistent dynamic model from segmented human magnetic resonance (MR) data and used it for EIT simulations. In particular, three scenarios, each one depicting a specific cardiac behaviour, were simulated. In one scenario, impedance changes were induced by blood volume variations only. In a second scenario, impedance changes were induced by the heart's motion only. Finally, in a third scenario, impedance changes were induced by both, blood volume variations and heart motion. The objective was to isolate and quantify the effect of each factor on the global cardiac impedance change. This whole process is described in more details in Section 2. The simulation results are provided in Section 3 and analysed in Section 4.

2 MATERIALS AND METHODS

The MR data acquisition is detailed in Section 2.1. Section 2.2 describes the creation process of our 2D dynamic bio-impedance model. Finally, the EIT simulations and image reconstruction details are provided in Section 2.3.

2.1 MRI Acquisition

The subject enrolled in this experiment was an 83-kg, 183-cm tall 50-year-old male with an underbust girth of 100 cm. MR images were acquired with a 3T Philips Achieva instrument. ECG-gated breath-held scans were performed in an oblique plane along the heart's long axis. A full cardiac cycle was imaged with a temporal resolution of 43 ms, resulting in a total of 20 2D image slices. The spatial resolution in the medial-lateral and anterior-posterior directions was 0.94 mm/pixel, and slice thickness 8 mm.

2.2 EIT Model Creation

2.2.1 Mr Data Segmentation

The cardiac cavities (atria and ventricles) and the myocardium were segmented manually at each of the 20 frames of the cardiac cycle in the MR images. The lungs, the pericardium, the descending aorta, the skeletal muscle, the spine and the thorax contour were segmented manually in the first frame only. The resulting segmentation can be seen in the top panel of Figure 1 (for one frame of the cardiac cycle).

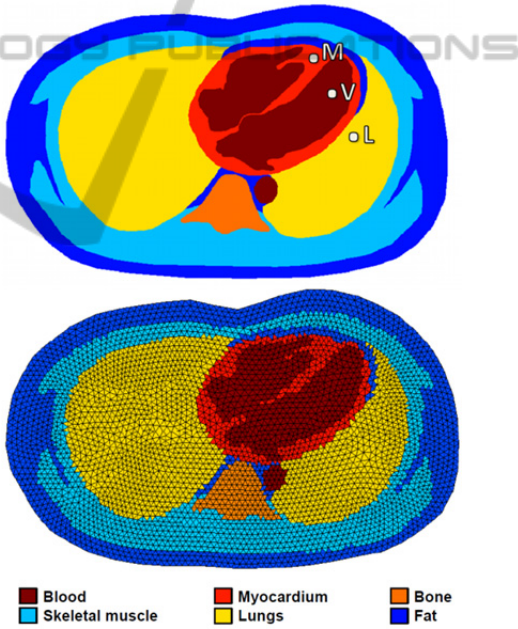

Figure 1: Top panel – Example of a segmented frame. The highlighted myocardial (M), ventricular (V) and anterior lung (L) locations will be used in Section 3. Bottom panel – The corresponding bio-impedance mesh for EIT simulations.

2.2.2 Model Assumptions

The following assumptions were made in the creation of our model following today's standard for 2D EIT:

- Electrical currents travel within the volume scanned by the MR instrument;

- Organs and tissues are isotropic (Guha, 1973);
- The reactive part of the impedance of organs and tissues is negligible in the EIT frequency range (Malmivuo, 1995). Similarly, magnetic effects can be neglected at those frequencies (Holder, 2005);
- The thorax contains no internal current sources (Holder, 2005);
- All points on the body surface in contact with an electrode have the same potential as the electrode and at all other surface points the electrical potential gradient normal to the surface is zero (Guha, 1973). Under these two boundary conditions, the generalized Laplace's equation governing the domain of interest has a unique solution (Kim, 1988).

2.2.3 Bio-impedance Mesh Generation

An extruded mesh of tetrahedral elements was generated using NETGEN and the open source EIDORS toolbox (Grychtol, 2012), and fits the subject's thorax contour in the scanned oblique plane. At each frame of the cardiac cycle, each finite element was assigned an electrical conductivity value of the organ or tissue it belonged to in the time laps of the current frame. The biological values of electrical conductivity used in this model are listed in Table 1.

Table 1: Tissue conductivities for an excitation frequency of 200 kHz (Gabriel, 1996).

Tissue	*Conductivity ($S \cdot m^{-1}$)*
Blood	7×10^{-1}
Skeletal muscle	4×10^{-1}
Myocardium	2.5×10^{-1}
Lungs (inflated)	8.5×10^{-2}
Bone	8.5×10^{-2}
Fat	2.5×10^{-2}

2.3 EIT Simulations

2.3.1 Simulated Scenarios

Three different 2D dynamic meshes were created, each depicting a specific cardiac behaviour:

- *Scenario A.* Only the dynamics of the filling and emptying cardiac cavities are used in this model while the myocardium remains static throughout the whole cardiac cycle (the same segmentation is used for all frames, thereby suppressing other changes). Similarly, all other organs and tissues remain static for all frames. Therefore, this scenario simulates blood volume-related impedance changes only.
- *Scenario B.* Only the dynamics of the myocardium is maintained in this model. The cardiac cavities remain static throughout the whole cardiac cycle (the same segmentation is used for all frames, thus suppressing other changes). Similarly, all other organs and tissues remain static for all frames. Therefore, this scenario simulates cardiac motion-induced impedance changes only.
- *Scenario C.* The dynamics of both, the cardiac cavities and the myocardium are simulated in this model. All other organs and tissues remain static throughout the whole cardiac cycle. Therefore, this scenario simulates both blood volume-related and motion-induced impedance changes.

Modelling variations in blood volume and heart motion separately allows isolating and thus quantifying the effect of each one of these factors affecting the global cardiac impedance change.

2.3.2 Image Sequences Reconstruction

EIT reconstruction is a severely ill-conditioned inverse problem. The diffusive nature of electrical current propagation only adds up to the complexity. Obtaining absolute impedance values in EIT is not only of great difficulty, but not necessary for most EIT-based biomedical applications, which are more interested in *functional* information (namely, the variation of impedance around a reference baseline value) (Denai, 2010). For this reason, *difference* EIT is typically used. Instead of directly considering the voltage measurements $\boldsymbol{v}$ and the conductivity distribution $\boldsymbol{\sigma}$, it makes use of difference data $\boldsymbol{y} = \boldsymbol{v} - \boldsymbol{v}_r$, where $\boldsymbol{v}_r$ is a reference set of voltages typically obtained by averaging the measurements of the first frames of an EIT recording. It corresponds to the so-called background conductivity distribution $\boldsymbol{\sigma}_r$, used to define the difference conductivity distribution $\boldsymbol{x} = \boldsymbol{\sigma} - \boldsymbol{\sigma}_r$. As a result, linear EIT reconstruction can be represented by an inverse matrix $\mathbf{R}$, which translates difference measurements $\boldsymbol{y}$ into a difference conductivity image $\hat{\boldsymbol{x}}$:

$$\hat{\boldsymbol{x}} = \mathbf{R}\boldsymbol{y} \quad (1)$$

The computation of the inverse matrix $\mathbf{R}$ depends on the reconstruction method. In that context, the GREIT algorithm (Adler, 2009) distinguishes itself by encoding performance requirements directly within the inverse matrix. In particular, $\mathbf{R}$ is pretrained by optimizing several figures of merit such as amplitude response and position error.

Evaluating how much blood volume variations and heart motion affect – particularly in terms of amplitude – the the global cardiac impedance signal,

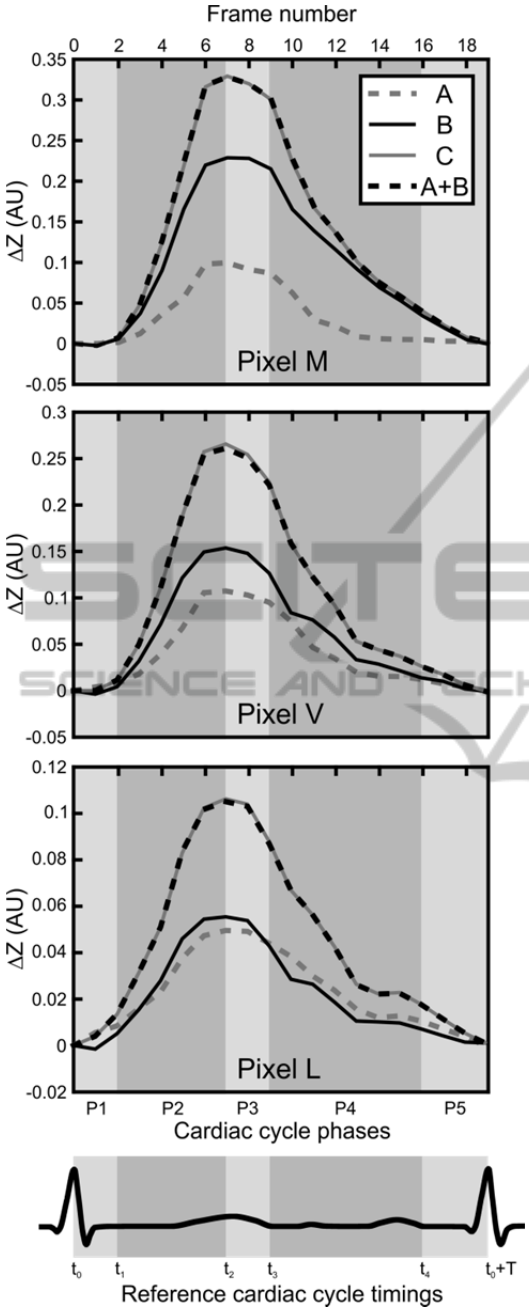

Figure 2: Impedance change occurring at the myocardial (M), ventricular (V) and anterior lung (L) pixels for all scenarios including the control scenario. A schematic ECG is also displayed as an illustrative timing reference. The meaning of the cardiac phases P1 to P5 (light and dark grey areas) and their associated reference timings t_0 to t_4 is detailed in Section 4.

requires such performance criteria to be optimal. Consequently, the GREIT algorithm was used to perform EIT simulations for each of the three specific scenarios described in Section 2.3.1. Difference data were obtained by using the first frame (representing the end of diastole) as reference data set. Each simulated scenario (*A, B* and *C*) resulted in a 20-frame sequence of 60 × 40 pixel images.

2.3.3 Control Scenario

An injected electrical current flowing through the heart will sequentially go through tissues belonging to the cardiac cavities and the myocardium, similarly to a current flowing through impedances connected in series. As a consequence, the impedances of scenario *C* should theoretically be similar to the sum of the impedances of scenarios *A* and *B*, since it encompasses both of their respective behaviours (blood volume-related impedance changes and motion-induced impedance changes). For this reason, a control scenario (scenario *A*+*B*) was virtually created by summing the image sequences reconstructed in scenarios *A* and *B*. It is expected to behave similarly to scenario *C*.

3 RESULTS

Figure 2 illustrates, for all scenarios (*A, B* and *C*) as well as the control scenario *A*+*B*, the impedance changes occurring at the myocardial (M), ventricular (V) and anterior lung (L) pixels shown in Figure 1.

Figure 3a illustrates the peak systolic impedance value (value at frame 7) for all scenarios, including the control scenario, at the myocardial (M), ventricular (V) and anterior lung (L) pixels, while Figure 3b illustrates the percentage of contribution of blood volume-related (scenario *A*) and motion-induced (scenario *B*) impedance changes to the global impedance change (scenario *C*).

4 DISCUSSION

Three different scenarios were investigated to evaluate the influence of blood volume changes and heart motion on the EIT cardiac signals. A 2D dynamic bio-impedance model was created from the segmentation MR images. Three cardiac behaviours – namely, blood volume-related (scenario *A*), motion-induced (scenario *B*) or both blood volume-related and motion-induced (scenario *C*) impedance changes – were simulated, and EIT image sequences reconstructed. A control scenario *A*+*B* was created virtually by summing the image sequences of the first two scenarios.

In the following discussion, we first verify the validity of the impedance waveforms observed at three specific pixel locations (Section 4.1). We then investigate the influence of each impedance-affecting factor to the global cardiac EIT signal (Section 4.2). Finally, we highlight some limitations of our model and suggest some possible future investigations (Section 4.3).

4.1 Impedance Waveforms Morphology Validation

A standard cardiac cycle can be subdivided into two isovolumetric phases (P1 and P3 in Figure 2), during which blood volume remains constant in the ventricles, and three anisovolumetric phases (P2, P4 and P5), during which changes in blood volume occur.

In scenario *A* (dashed grey curves in Figure 2), the only impedance-affecting factor is the change in blood volume induced by volume variations of the cardiac cavities. Shortly after the R peak of the ECG (at time t_0, corresponding to frame 0 in Figure 2), the first isovolumetric phase (P1) begins. No variation in blood volume occurs and thus the impedance waveform remains flat. When the semilunar valves open at $t_1 \approx t_0 + 80$ ms (Levick, 2010) (corresponding to frame 2), the first anisovolumetric phase (ventricular ejection) starts, and blood volume decreases in the cardiac cavities (phase P2 in Figure 2). The heart thus becomes less conductive and its impedance increases steeply. A short isovolumetric relaxation phase follows (P3). At $t_3 \approx t_0 + 440$ ms (Levick, 2010) (frame 9), when the atrioventricular valves open, the ventricular volume starts returning (rapidly at first, then slowly) to its baseline value as ventricular filling begins (phase P4 in Figure 2). At the start of atrial systole at $t_4 \approx t_0 + T - 160$ ms (Levick, 2010) (frame 16), where T is the cardiac period, ventricular blood volume increases slightly while atrial volume decreases by the same amount, thus not influencing significantly the global impedance change (phase P5 in Figure 2).

In scenario *B* (solid black curves in Figure 2), only the dynamics of the myocardium are simulated. The remaining organs and tissues remain static. This scenario thus simulates motion-induced impedance changes. During ventricular systole (phase P2 in Figure 2), longitudinal shortening of the myocardium begins as the apex is pulled towards the atrioventricular plane. The space occupied by the myocardium during diastole becomes occupied by the pericardium, the conductivity of which is ten times smaller than that of the cardiac muscle (Table 1). As a result, impedance increases abruptly. As the semilunar valves close, the myocardium undergoes elastic recoil and starts reoccupying the space it left during ventricular systole, thus producing an impedance decrease (phase P4 in Figure 2). The synchrony between the waveforms of scenarios *A* and *B* relates on the one hand to the simultaneous beginning of the ejection phase and the myocardial contraction, and on the other hand to the fact that the opening of the atrioventricular valves (and thus ventricular refilling) is caused by a sharp decrease in pressure due to myocardial relaxation (Levick, 2010).

In scenario *C* (solid grey curves in Figure 2), which aims at reflecting the real behaviour of the heart, the dynamics of both, the cardiac cavities and the myocardium are maintained to simulate both, blood volume-related and motion-induced impedance changes. The remaining organs and tissues are static. As the strong similarity between the solid grey and dashed back curves (scenario *C* and control scenario *A*+*B*) of Figure 2 illustrates, the contributions of blood volume variations and heart motion add up to produce the impedance changes observed in scenario *C*.

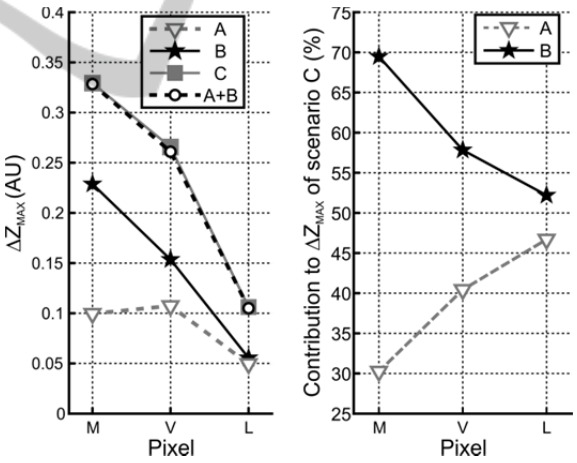

Figure 3: Left panel – Peak systolic impedance value for all scenarios, including the control scenario, at the myocardial (M), ventricular (V) and anterior lung (L) pixels. Right panel – Contribution of blood volume-related (scenario *A*) and motion-induced (scenario *B*) impedance changes to the global impedance change (scenario *C*). These percentages were computed as the ratio of the peak systolic values of scenarios *A* and *B* (Figure 3a) with those of scenario *C*.

4.2 Influence of each Factor Affecting Impedance

The impedance changes occurring at three different

anatomical locations (M, V and L, depicted in Figure 1) were investigated. The resulting impedance waveforms are shown in Figure 2. It is worth noting that the diffusive nature of electrical current propagation makes the mapping of function onto anatomy challenging (*i.e.* a pixel identified as belonging to a given organ or tissue using MR information does not necessarily only reflect the functional impedance information of the said organ or tissue). For instance, our anterior lung pixel (L) is expected to be slightly affected by both, cardiac blood volume-related and motion-induced impedance changes, because of its proximity to both sources of perturbations. Similarly, motion-induced impedance changes are expected to be larger in the myocardial (M) pixel than in the ventricular (V) pixel. The opposite is expected for blood volume-related changes.

These assumptions are confirmed in Figure 3a, which illustrates how the amplitude of motion-induced impedance changes (scenario *B*) decreases as one moves away from the heart's long axis (away from pixel M). Conversely, the amplitude of blood volume-related impedance changes (scenario *A*) is maximal when measured in the ventricular pixel (V). The amplitude of the impedance change in the anterior lung pixel (L) is significantly smaller for both factors. It would be interesting in a future study to compare this amplitude to that of impedance changes of pulmonary origin to assess the level of perturbation caused by cardiogenic impedance variations on the neighbouring lung region.

Figure 3b quantifies the influence of each factor to the cardiac EIT signal. Based on these simulations, it appears that in the myocardial (M) and in the ventricular (V) pixels the signal is dominated by impedance changes originating from the heart's motion. In the anterior lung pixel (L) the influence of both factors is approximately the same. According to our model, it thus appears that the impedance change originating from the heart's motion is the main factor affecting the global cardiac impedance change.

4.3 Limitations

Our observations have provided novel insights into the understanding of the genesis of cardiac impedance changes in EIT. However, these results necessitate further investigations, as they are based on a simplified simulation model showing three main limitations:

- The model is two-dimensional, while electrical currents are known to propagate in three dimensions. Impedance changes occurring above and below the electrode plane are thus not considered adequately.
- The blood volume variations and the motion of the remaining organs and tissues are not modelled. In particular, the influence of respiratory movements, pulmonary perfusion and blood volume changes in the major elastic arteries, is not taken into account. While this allows isolating the influence of each individual factor in simulations, it neglects their interdependencies acting in reality.
- Only one subject was used in our experiment.

5 CONCLUSIONS

We developed a 2D dynamic bio-impedance model for EIT simulations. Our study shows that EIT signals in the heart area might be dominated by motion-induced impedance changes.

Based on these important observations, it would be interesting to investigate possible solutions, such as exploiting larger frequency content or a multi-frequency approach to perform source separation, or enhancing the EIT signals using motion-compensating models. It is worth mentioning that these approaches could be exploited either before or after image reconstruction.

Additionally, experimental and clinical studies should be performed to confirm what we observed in our model.

ACKNOWLEDGEMENTS

This work was made possible by grants from the SNSF/Nano-Tera.CH's project OBESENSE (20NA21-1430801).

REFERENCES

Adler, A., Arnold, J. H., Bayford, R. et al., 2009. *GREIT: a unified approach to 2D linear EIT reconstruction of lung images*, Physiological Measurement, vol. 30, no. 16, pp. S35–S55.

Barber, D. C., 1990. *Quantification in impedance imaging*, Clinical Physics and Physiological Measurement, vol. 11 (suppl A), pp. 45-56.

Bayford, R. H., 2006. *Bioimpedance tomography (electrical impedance tomography)*, Annual Review of Biomedical Engineering, vol. 8, pp. 63-91.

Borges, J. B., Suarez-Sipmann, F., Böhm S. H. et al., 2011. *Regional lung perfusion estimated by electrical*

impedance tomography in a piglet model of lung collapse, Journal of Applied Physiology, vol. 112, no. 11, pp. 225-236.

Braun, F., 2013. *Systolic Time Intervals Measured by Electrical Impedance Tomography (EIT)*, Swiss Federal Institute of Technology, Zurich, Switzerland. DOI: http://dx.doi.org/10.3929/ethz-a-009947722.

Brown, B.H., Leathard, A., Sinton, A. et al., 1992. *Blood flow imaging using electrical impedance tomography*, Clinical Physics and Physiological Measurement, vol. 13 (suppl A), pp. 175-179.

Deibele, J. M., Luepschen H. and S. Leonhardt, 2008. *Dynamic separation of pulmonary and cardiac changes in electrical impedance tomography*, Physiological Measurement, vol. 29, no. 16, pp. S1-S14.

Denai, M. A., Mahfouf, M., Mohamad-Samuri, S. et al., 2010. *Absolute Electrical Impedance Tomography (aEIT) Guided Ventilation Therapy in Critical Care Patients: Simulations and Future Trends*, IEEE Transactions on Information Technology in Biomedicine, vol. 14, no. 13, pp. 641-649.

Fagerberg, A., Stenqvist, O. and Åneman, A., 2009. *Monitoring pulmonary perfusion by electrical impedance tomography: an evaluation in a pig model*, Acta Anaesthesiologica Scandinavica, vol. 53, no. 12, pp. 152-158.

Ferrario, D., Grychtol, B., Solà, J. et al., 2012. *Towards morphological thoracic EIT: Major signal sources correspond to respective organ locations in CT*, IEEE Transactions on Biomedical Engineering, vol. 59, no. 111, pp. 3000-3008.

Frerichs, I., Hinz, J., Herrmann, P. et al., 2002. *Regional lung perfusion as determined by electrical impedance tomography in comparison with electron beam CT imaging*, IEEE Transactions on Medical Imaging, vol. 21, no. 16, pp. 646-652.

Frerichs, I., Pulletz, S., Elke, G. et al., 2009. *Assessment of changes in distribution of lung perfusion by electrical impedance tomography*, Respiration, vol. 77, no. 13, pp. 282-291.

Gabriel, S., Lau, R. W. and Gabriel, C., 1996. *The dielectric properties of biological tissues: III. Parametric models for the dielectric spectrum of tissues*, Physics in Medicine and Biology, vol. 41, no. 111, pp. 2271–2293.

Grant, C. A., Pham, T., Hough, J. et al., 2011. *Measurement of ventilation and cardiac related impedance changes with electrical impedance tomography*, Critical Care, vol. 15, no. 11, p. R37.

Grychtol, B., Lionheart, W. R. B., Bodenstein, M. et al., 2012. *Impact of Model Shape Mismatch on Reconstruction Quality in Electrical Impedance Tomography*, IEEE Transactions on Medical Imaging, vol. 31, no. 19, pp. 1754-1760.

Guha, S. K., Khan, M. R. and Tandon, S. N., 1973. *Electrical field distribution in the human body*, Physics in Medicine and Biology, vol. 18, no. 5, pp. 712-720.

Hellige, G., Hahn, G., 2011. *Cardiac-related impedance changes obtained by electrical impedance tomography: an acceptable parameter for assessment of pulmonary perfusion?,* Critical Care, vol. 15, p. 430.

Holder, D. S., 2005. *Electrical impedance tomography: methods, history and applications*, Institute of Physics Publishing. London.

Kim, D. W., Baker, L. E., Pearce, J. A. and Kim, W. K., 1988. *Origins of the impedance change in impedance cardiography by a three-dimensional finite element model*, IEEE Transactions on Biomedical Engineering, vol. 35, no. 112, pp. 993-1000.

Kunst, P. W. A., Vonk-Noordegraaf, A., Hoekstra, O. S. et al., 1998. *Ventilation and perfusion imaging by electrical impedance tomography: a comparison with radionuclide scanning*, Physiological Measurement, vol. 19, no. 14, pp. 481–490.

Leathard, A. D., Brown, B. H., Campbell, J. et al., 1994. *A comparison of ventilatory and cardiac related changes in EIT images of normal human lungs and of lungs with pulmonary emboli*, Physiological Measurement, vol. 15 (suppl 2A), pp. A137-A146.

Levick, J. R., 2010. *An introduction to cardiovascular physiology*, Arnold. London, 5th edition.

Malmivuo, J. and Plonsey, R., 1995. *7: Volume source and volume conductor*, in Bioelectromagnetism: Principles and Applications of Bioelectric and Biomagnetic Fields, University Press. New York.

McArdle, F. J., Suggett, A. J., Brown, B. H. and Barber, D. C., 1988. *An assessment of dynamic images by applied potential tomography for monitoring pulmonary perfusion*, Clinical Physics and Physiological Measurement, vol. 9 (suppl A), pp. 87-91.

Nguyen, D. T., Jin, C., Thiagalingam, A. and McEwan, A. L., 2012. *A review on electrical impedance tomography for pulmonary perfusion imaging*, Physiological Measurement, vol. 33, no. 5, pp. 695–706.

Smit, H. J., Vonk-Noordegraaf, A., Marcus, J. T. et al., 2004. *Determinants of pulmonary perfusion measured by electrical impedance tomography*, European Journal of Applied Physiology, vol. 92, no. 1, pp. 45-49.

Vonk-Noordegraaf, A., Kunst, P. W. A., Janse, A. et al., 1998. *Pulmonary perfusion measured by means of electrical impedance tomography*, Physiological Measurement, vol. 19, no. 12, pp. 263–273.

Vonk-Noordegraaf, A., Janse, A., Marcus, J. T. et al., 2000. *Determination of stroke volume by means of electrical impedance tomography*, Physiological Measurement, vol. 21, no. 12, pp. 285–293.